

# Global Dust Deposition with Orac

D.J.Fulton\*

October 11, 2017

## Abstract

This report details work carried out by myself in summer 2017 within the AOPP summer vacation studentship under the supervision of Adam Povey and Don Grainger. This report concerns the deposition of aerosol dust from the atmosphere to the earth surface. In this work I lay out the history of calculating dust deposition rate through different methods. I chose a method of calculation with minimal assumptions which combines the CALIOP lidar data for dust profile, the ORAC dust aerosol AOD for total column mass, and the ECWMF interim wind data for mass flow. I find that calculating the dust deposition and source rates was limited in extent by the coverage of the ORAC dust aerosol data and to a lesser extent by the CALIOP lidar data and I find that the uncertainty was largely dominated by the dust profile. What I have achieved is seasonal dust deposition maps for the overlapping period of the 3 datasets with the ability to project deposition backwards as far as 1995. The magnitude of dust deposition globally was found to be on the order of  $0.1Tg\ month^{-1} (1^\circ \times 1^\circ)^{-1}$  with a high production in the Sahara region. However, it must be noted that the analysis of the data produced some spurious features such as dust emission from remote ocean regions.

---

\*djamesfulton@yahoo.co.uk

# 1 Introduction

The deposition of mineral dust across the earth's oceans, seas and land masses is of particular scientific interest due to the potential of this substance to act as a natural fertiliser. It has been proposed that deposition of dust aerosol is the mechanism by which the Amazon basin maintains its fertility [1]; this is required to balance hydrological loss of phosphorus. It is also predicted that the influx of nutrients from dust deposition is key to algae blooms and phytoplankton in global seas and oceans [2, 3, 4, 5, 6, 7]. There have been suggestions that iron may be the limiting factor in phytoplankton growth in up to 30% of the earth's oceans in high nutrient low chlorophyll regions. There has been studies, such as [8], which show correlation between the deposition of aerosol and chlorophyll blooms. The last mentioned study suggests that in the Greenland seas, aerosol is a more dominant forcing on phytoplankton than even sea ice coverage.

# 2 Literature Review

There have been many attempts to characterise the deposition rate of atmospheric mineral dust to the earth's surface. In [9] they use collect individual air samples which are later analysed in a laboratory setting to find the local dust aerosol mixing ratio in air. This is then extrapolated, with approximation, to estimate the iron deposition in the north Atlantic. This study introduces one of the main problem areas in calculating the flux into the ocean; that is that it is relatively easy to establish the concentration of mineral aerosols in the air but it is then much harder to quantify with any certainty the transfer rate between these suspended aerosols and the earth's surface. The rate at which the suspended minerals are deposited is quantified by their *deposition velocities*. This quantity is poorly defined and is subject to uncertainty factor of around 3.

The reader should be familiar with [10] as a significant early work in trying to estimate aerosol deposition. In that paper the difficulties of estimating the deposition velocity are laid out. The main problem we have is that of dry deposition, deposition which occurs without the effects of precipitation. Wet deposition, where aerosol is rained-out (or through any other form of precipitation) is much easier to quantify since one simply needs to collect precipitation samples, find the aerosol mass contained in the sample, and collate this with the local precipitation rate and aerosol concentration. Once a rain-out factor is achieved we can use it in a bulk sense by considering precipitation and aerosol concentration globally. This method lacks finesse in that it ignores any structure in the column distribution of aerosol above the surface and cloud aerosol interaction, it remains blind to these effects and just takes a statistical average; however it is still better quantified than that of dry deposition. Dry deposition is most important for large particle sizes, particularly mineral dust and marine salt spray. There have been efforts to quantify dry deposition by creating surrogate surfaces. The easiest earth surface to imitate may be that of the open ocean; one simply needs to set up a tank of ocean water through which we can collect deposited sediment after some period of time. This experiment has been run by installing such a collecting tank on a research vessel; however there remain questions about how much this limited collecting surface will mimic a large open ocean. The differences one might consider may be the motion of the water surface, and the effects of deposited material concentration within the water on settling velocity. The former of these points may have a significant effect since in open ocean we expect sediment to sink and the higher the material concentration is on the surface of the tank the larger we expect the loss of material back into the atmosphere. Therefore a shallow surrogate ocean is unlikely to represent well the open ocean.

This then puts a lot of uncertainties on the figures achieved via measuring the in situ the concentration of aerosol at the ocean surface and using some bulk parameter, the deposition velocity, to estimate the expected flow into the oceans. The same uncertainty is again raised when we use models to calculate the deposition (such as in [11]) since these models must themselves include deposition velocities for each surface. However, many of these models are of interest and perhaps they present the best estimate of the mineral deposition that we can make right now considering the data that is

currently available. One study, [12], which compares the dust deposition rate calculated by 15 different models found that they returned depositions consistent within a factor of 10. Of course combining the results of multiple models is more reliable than relying on any single one, but systematic errors may still exist.

There is one more method one can utilise in calculating the dust deposition rate globally, and this is the one that I have chosen to investigate in this study. This method combines observational data of dust aerosol along with the simple principle of conservation of mass. A formative work of this method, [13], was accomplished by Kaufman et al.; this procedure has been investigated several more times since in varying complexity [14, 15, 16, 17, 18]. The lattermost of these studies presents a good outline of the limitations of earliest study by Kaufman.

### 3 Methods - Datasets Used

To carry out the deposition calculations we need four key datasets which vary in space and time. These are; the absolute magnitude of the dust AOD (Aerosol Optical Depth) at each lat-lon coordinate,  $A_{ij}(t)$ ; the normalised extinction profile at each lat-lon and altitude,  $\hat{b}_{ijk}(t)$ , this tells us how the aerosol is dispersed within each vertical air column; the eastwards and northwards wind velocities at each lat-lon and altitude,  $U_{ijk}$  and  $V_{ijk}(t)$ ; and finally the mass extinction efficiency,  $\Omega$ .

With these quantities we can estimate the flow of mass into and out of each column of air, and then take the divergence of the flow to be the deposition (see equation (4)). This avoids the problem of quantifying the deposition velocity and instead we use the conservation of mass to calculate deposition.

#### 3.1 The Mass Extinction Efficiency

One of the major considerations in this method is in the value of the mass extinction efficiency,  $\Omega$ . Not only is it subject to uncertainty in its value but there is likely to be a spatial and temporal variation in this quantity in the actual global dust plumes, [19]. The reason for this variability is that the aerosol particle size distribution is different based on the distance to the particle source; there are more large particles close to the source than further from the source since larger particles are more susceptible to gravitational settling. This can be seen from the particle size distribution measured downwind of the Sahara measured using sediment traps in [19, 20]. Also, the average geometry of particles is likely to become less spherical downwind, since spherical particles have a larger deposition velocity, [21]. This in turn has an effect the mass extinction efficiency.

Ultimately the figure I chose came from experimental data summarised in [22]. The reported experimental data in the study gave a value of  $\Omega = 0.53 \pm 0.02m^2g^{-1}$  which doesn't agree with the OPAC model theoretical value of  $0.64m^2g^{-1}$ . This presents a source of inconsistency in the analysis because the ORAC data was extracted from observations using the properties predicted by the OPAC model. I was unsure how this choice would affect the results with respect to reality; we have seen that the OPAC model does not accurately predict the mass extinction efficiency of dust aerosol by comparing the OPAC  $\Omega$  to the experimental  $\Omega$ . It could be that the choice made is the incorrect one and that whatever systematic error introduced in extracting the ORAC data from observation would be reduced by using the OPAC  $\Omega$ ; on the other hand, this choice may compound the systematic error, so the best choice would be the experimental  $\Omega$ .

This choice affects the absolute magnitude of mass deposition, with the experimental  $\Omega$  giving a mass deposition rate about 20% higher than the OPAC prediction. However, neglecting the importance of this choice; noting that models vary in their predictions by a factor of 10, and noting that whichever of the two values we pick will still be incorrect in some areas of the globe because we expect  $\Omega$  to vary spatially and seasonally; we can still extract some information about the magnitude of deposition and its spatial variation. The value chosen for  $\Omega$  (assuming we are limited to choose a single value rather than a spatially varying field), will not affect the outcome of the spacial distribution of deposition, merely the magnitude.

We note that the absence of any study aiming to quantify the spatial and seasonal variation of  $\Omega$  is a detriment to this work. I wonder if some small improvement could be made by collating together the results of sediment trap studies to estimate the spatial variance downwind of dust sources, this could be possible since some sediment trap studies report the distribution of particle sizes measured.

### 3.2 Aerosol Optical Depth

This quantity was taken from the Aerosol CCI ORAC Level 3 v4.01 monthly dataset. Therefore what we will be representing by  $A_{ij}(t)$  will be the average monthly aerosol optical depth at each lat-lon gridpoint. I chose to take the monthly average as there is a significant limit the coverage available on each individual day. In theory it would be good if we could use AOD on a daily level since much of the dust deposited in the oceans can come from short lived dust plumes which have a lifetime much shorter than a month. For these significant events we would wish to see where the plumes are deposited. However, since the goal of this work is to find more long term averages on dust deposition, in seasonal and yearly trends, as long as these short lived dust plumes are taken into our averages of AOD and so long as these plumes are not accompanied by wind velocities which are significantly different from their monthly averages, it is unlikely that these plumes will have a very large effect on the accuracy of our estimates.

### 3.3 Extinction Profile

This kind of dataset was not globally available at the time of Kaufman’s initial study, but now, following several years of the CALIOP instrument, we have access to these profiles globally for the period post-2006. This extinction profile is extracted using lidar which allows us to see not only the absolute magnitude of AOD, but how the the optical depth gradient changes with altitude. After private communication with Adam Povey I was led to believe that this dataset was reliable for the dispersion of aerosol throughout the air column but that the absolute magnitude did not represent the true total AOD as well as an instrument such as ASTR from which ORAC is extracted. Therefore the CALIOP profiles were extracted and normalised so that it was possible to distribute the ORAC derived AOD at various altitudes in the atmosphere. The data used was the *CAL\_LID\_L3\_APro\_CloudFree-Standard-V3-00* version.

The extinction coefficient  $b$  is related to the attenuation of light via

$$\frac{dI}{dz} = -bI, \quad (1)$$

where  $I$  is the intensity of the light and  $z$  the distance through the material. The extinction coefficient is also related to AOD via

$$A_{ij} = \int_0^H b_{ij}(z) dz \quad (2)$$

where  $H$  is the height of the atmosphere. The dataset available from the CALIOP instrument is not exactly  $b_{ij}(z)$  but it is  $b_{ijk} = b_{ij}(z_k)\delta z_k$ , where  $A_{ij} = \sum_{k=0}^N b_{ijk}$  and  $\delta z_k$  is the spacing between altitudes at index  $k$ .

### 3.4 From Aerosol Optical Depth to Column Mass

It is very trivial to go from AOD to the equivalent surface density of aerosol in a column once you have established the value of the mass extinction efficiency. The equation linking the two of them is simply,

$$M_{ij} = \frac{A_{ij}}{\Omega}. \quad (3)$$

The only thing that may be of interest is the wavelengths that each of our results were calculated at. Our of value of  $\Omega$  is reported in the region of 500-550nm;  $b_{ijk}$  is presented for 532nm and  $A_{ij}$

is presented at 550nm. This study was carried out at the native wavelength of ORAC, 550nm. In principle we could have interpolated the CALIOP extinction profiles to this wavelength using the angstrom exponent. However, since we wish to take a normalised profile from these profile there was little point. It would simply mean we would apply a different scaling coefficient to them later.

### 3.5 Wind Velocity

These datasets for  $U_{ijk}(t)$  and  $V_{ijk}(t)$  were taken from the ECMWF ERA-Interim synoptic monthly averages. I extracted the wind speeds in the easterly and northerly directions at all model levels along with the supplied geopotentials. As is common, I assumed geopotential height to be essentially equivalent to altitude in further calculations.

A consideration that one needs to make is whether the aerosol moves at the same velocity as the wind. This is logically obvious by considering the fact that the aerosols are suspended in the air by their interaction with it, through essentially the action of Brownian motion. However in [23] it was found that the observed progression of dust fronts as measured via satellite images from MODIS Aqua and Terra was systematically faster than the NCEP predicted windspeeds at the same time. In short this study showed that the dust moved faster than the wind.

There are many explanations one could consider to accommodate this difference, first amongst them being the accuracy of the NCEP wind database, but this is beyond the scope of this study. For now it may help to think of an inertial parcel of air into which we project aerosol particles. We would expect, through friction, that these aerosol particles must slow down and stop any bulk motion with respect to the air. Thereby becoming stationary in the frame of reference of the parcel of air. We will use this thought experiment as justification that on mass we expect aerosol particles to move with the same velocity as the surrounding air, albeit with some downwards settling velocity.

## 4 Methods - Stitching the data together

In this section I will lay out the method by which I combine these data into a final result, dealing with all issues that appear on the way towards this. Towards the end of this section I will discuss the error analysis and the limitations of this as well as the dominant source of error.

### 4.1 Differing Coordinate Basis

The three different datasets for AOD, extinction profile and wind velocities each come with their own coordinate basis. The lat-lon components of these basis are summarised in the figure below where  $n$  and  $m$  represent integer degree longitudes and latitudes. We can see from the figure that we will need to interpolate and fill values to allow us to use this data together. I chose to perform the analysis at the lat-lon scale of the Orac data, with each latitude point centred on  $m + \frac{1}{2}^\circ$  and each longitude point centred on  $n + \frac{1}{2}^\circ$  for  $m \in [-90...89]$  and  $n \in [-180..179]$ . This required us to assume the CALIOP derived extinction profile to be invariant in the region covered by the blue rectangle in figure 4.1. This was essentially a nearest neighbour filling approach. Thought was given as to whether this was the most valid approach, particularly contrasting this to some interpolation method that could have been used, but because each CALIOP measurement is the average of measurements taken within each cell represented by the blue rectangle of the figure I supposed that the true value of each profile within a  $1^\circ \times 1^\circ$  square was used in calculating the average profile over the CALIOP rectangle. Therefore nearest neighbour was adopted. The ECMWF wind data was offset to the ORAC derived data by  $0.5^\circ \times 0.5^\circ$  in lat-lon. To account for this I adopted a linear interpolation which, because of the spacing of the two datasets, was equivalent to taking the average of the 4 nearest neighbours to the ORAC lat-lon gridpoints.

I also had to chose a vertical coordinate scale over which to perform the analysis. Note that both the ECMWF and CALIOP derived data include an altitude dimension whilst the ORAC data does

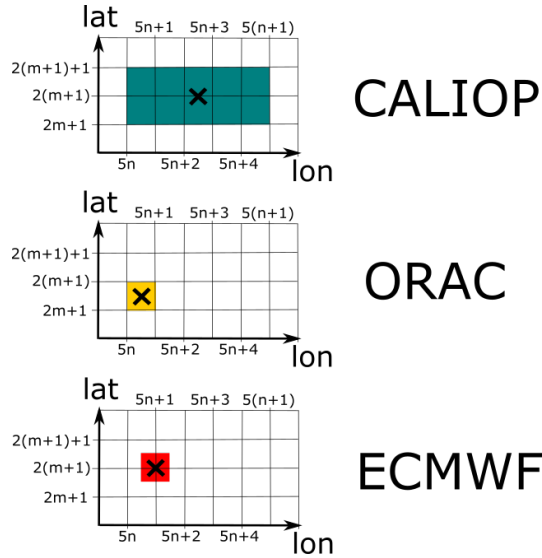


Figure 1: How the raw data coordinates overlap. The  $\times$  indicates a single sample coordinate placement in the spaces shown and the shaded region shows the space over which this point covers; i.e. where it is the closest given point.

not. I carried out the analysis at the height scale of the CALIOP data which is at a finer altitude resolution than the ECMWF wind data. To accommodate for this I applied a linear interpolation to the ECMWF data to transform it to the altitude scale of CALIOP. Note that this means that I performed two linear interpolations on the ECMWF data. This first interpolation was applied in the altitude dimension to change to the altitude scale of CALIOP. The second was a 2D interpolation to the lat-lon scale of ORAC. I noted that a better interpolation of the data would have been to do a 3D interpolation rather than the two interpolations described above. However, since the ECMWF data is naturally calculated in pressure levels and then transformed to geopotential height this means that it is not on a regular spacial grid. The lat-lon grid is uniform but the altitude coordinate is not. This fact makes the 3D interpolation more computationally heavy; but between neighbouring columns of air (those on neighbouring lat-lon points) there is generally only a small variation in the altitude values (significantly less than the altitude spacing). Therefore the error introduced by this two part interpolation will be small.

## 4.2 Calculating the Deposition

The total rate of aerosol flow into a lat-lon cell,  $F_{ij}$ , can be calculated as follows; where  $i$  is the index corresponding to latitude,  $j$  is the index corresponding to longitude and  $k$  is the index corresponding to altitude. Also note that in this calculation I defined the indices such that there was a wrap-around in the East-West direction, i.e., that the most easterly cell could exchange aerosol with the most westerly as long as they were at the same latitude. I did not allow for wrap-around over the north or south pole because the coverage of our data meant that we could not analyse these areas anyway (as will be seen later).

$$\begin{aligned}
F_{ij} = \frac{1}{\Omega} \{ & \\
& - \sum_k \left\| \oplus A_{i,j} \hat{b}_{ijk} U_{ijk} L_{ij}^{u+} \right\| + \left\| \ominus A_{i,j} \hat{b}_{ijk} U_{ijk} L_{ij}^{u-} \right\| + \left\| \oplus A_{i,j} \hat{b}_{ijk} V_{ijk} L_{ij}^{v+} \right\| + \left\| \ominus A_{i,j} \hat{b}_{ijk} V_{ijk} L_{ij}^{v-} \right\| \\
& + \sum_k \oplus A_{i-1,j} \hat{b}_{i-1,j,k} V_{i-1,j,k} L_{ij}^{v-} \\
& + \sum_k \ominus A_{i+1,j} \hat{b}_{i+1,j,k} V_{i+1,j,k} L_{ij}^{v+} \\
& + \sum_k \oplus A_{i,j-1} \hat{b}_{i,j-1,k} U_{i,j-1,k} L_{ij}^{u-} \\
& + \sum_k \ominus A_{i,j+1} \hat{b}_{i,j+1,k} U_{i,j+1,k} L_{ij}^{u+} \\
& \left. \right\}. \quad (4)
\end{aligned}$$

Where  $\oplus$  represents the operation of “add iff the term to follow is positive” and similarly  $\ominus$  represents the operation of “minus iff the term to follow is negative”. In this expression  $A_{ij}$  is the dust AOD at the grid index ij, where increasing i means moving Northwards and increasing j means moving eastwards. The index k is reserved for altitude and that is why we have a sum over it at all gridpoints. The normalised extinction profile is given the symbol,  $\hat{b}_{ijk}$ . It relates to the regular CALIOP extinction coefficient  $b_{ijk}$ , via

$$\hat{b}_{ijk} = \frac{b_{ijk}}{\sum_{jk} b_{ijk}} \quad (5)$$

Obviously  $U_{ijk}$  and  $V_{ijk}$  are the winds in the direction West→East and South→North respectively.  $\Omega$  is the mass extinction efficiency of the dust. Finally,  $L_{ij}^{u(v)\pm}$  represents the physical length of the side of the grid square against which the wind component u(v) is blowing. This length is measured perpendicular to the direction of flow of the wind and may have a different length  $L_{ij}^{u(v)-}$  or  $L_{ij}^{u(v)+}$  depending on whether the wind is blowing in the negative index direction (towards lower j(i)) or the positive index (towards higher j(i)) direction. This is only a small effect, and only applies in the North-South direction. If the latitudes are given symbol  $\theta_i$  and the longitudes given symbol  $\phi_j$ , then we can express  $L_{ij}^{u\pm} = \delta\theta R$ , and  $L_{ij}^{v\pm} = \delta\phi \cos(\theta_i \pm \delta\theta) R$ . Here  $R$  is the radius of the earth and  $\delta\theta$  and  $\delta\phi$  are the spacings of the latitudes and longitudes respectively on the regular grid.

Equation (4) above can be easily understood by thinking of a simple case of flow across a boundary. For an plane of area  $A$  through which a substance of density  $\rho$  is flowing as speed  $u$  perpendicular to the plane, the flow rate  $f = A\rho u$ . Equation (4) just builds up this logic where  $A \rightarrow L_{ij}^{u(v)\pm} \delta z_k$ ,  $\rho \rightarrow A_{ij} \frac{\hat{b}_{ijk}}{\Omega} \frac{1}{\delta z_k}$  and  $u \rightarrow U_{ijk}(V_{ijk})$ . The lines of equation (4) can be explained as such:

- Line 1 - Flow of aerosol mass out of the grid index ij
- Line 2 - Flow into index ij from index i-1,j. This is flow into square ij from its neighbour to the west.
- Line 3 - Flow into index ij from index i+1,j. This is flow into square ij from its neighbour to the east.
- Line 4 - Flow into index ij from index i,j-1. This is flow into square ij from its neighbour to the south.
- Line 5 - Flow into index ij from index i,j+1. This is flow into square ij from its neighbour to the north.

All of these are summed over the altitude index  $k$ .

We are performing this calculation with data which is averaged over the course of a month and so we assume this to be static and in equilibrium. Therefore, the total flow into a cell must be balanced by deposition within that cell, and so where  $F_{ij} > 0$  there is deposition of aerosol and where  $F_{ij} < 0$  there is aerosol being emitted, at the rate of  $|F_{ij}|$ . This quantity is in mass per unit time.

The advantages of this method are simple; the first is that the calculation is quite straight forward with just some specifics to work out; we also have assumed almost nothing except for that our raw data is reliable and that the aerosol moves at the same velocity as the wind. We have included only the North, South, East and West flow in/out of each cell but not vertical transport within the column. It would have been possible to add this consideration into our calculations with little effort since there are ECMWF vertical wind fields available; however since our ultimate goal is to find the mass flux divergence as a total throughout the column (i.e. how much mass appears or disappears inside the air column) and we are not interested at what height it disappears, we can ignore this term. These vertical flux terms cancel out throughout a column to give the same result.

### 4.3 Averaging Deposition

In the section above we saw the algorithm to calculate the aerosol flux into and out of each cell. Now we must talk about how we should average these over a period of time. The datasets of interest for ORAC represent a daytime monthly average of AOD, the datasets from ECMWF represent synoptic monthly averages of wind (average monthly winds at 06:00, 12:00, 18:00, 00:00) and the CALIOP datasets represent monthly extinction profile at either night or day. The last of these is of particular interest since it is a large source of uncertainty. The lidar measurements of CALIOP are generally better and with lower uncertainty at night time due to interference from sunlight during the day. This has led other studies similar to this one to chose the night time data only and assume the daytime data is the same. I have chosen not to do this, but instead to use both sets and combine them with the synoptic winds and daytime ORAC AOD. One can imagine that the dispersion of aerosol throughout the column may have quite different structure at day as compared to night. Then considering the diurnal cycle of winds at day or night, the flux between our grid cells is most likely going to have a day-night cycle as well (although I did not test this). If one thinks about how the total AOD may change from day to night it becomes clear that this should be less important than the dispersion, at least over open ocean.

Consider an average monthly night time AOD compared to an average monthly daytime AOD over open ocean. Taking the wind data and averaging at each height level, the maximum value of this quantity below  $8km$  altitude is  $70km\ h^{-1}$  which equates to roughly a  $10^\circ$  transport within 12 hours at the equator. So the night time range of aerosol is  $10^\circ$  at the equator. If there was some diurnal cycle in AOD, such as lots of deposition at night, we would still expect this to feed into a monthly average taken at daytime since if the distance from a aerosol source is greater than  $10^\circ$  there could not be a dip in AOD and then recovery to a daytime average value overnight. Therefore we use the ORAC daytime AOD as an alltime average. Noting is limitations, especially close to dust sources where there may be some diurnality to AOD.

Below, the table shows how the calculation for a month was made up of different pieces of the data available. It shows weighting factors and it is equivalent of taking daytime from 06:00-18:00 and night time otherwise.

## 5 Results and Discussion

Shown below in figures 2 and 3 are the average winter and summer dust aerosol deposition rates between 2006 and 2011. These were calculated by taking the overlap period between the ORAC and CALIOP data. We extracted depositions from each month in the overlap and took the average of the depositions for each season.

Table 1: Break down of the datasets combinations used, along with their weighting factors, in calculating monthly average deposition.

Component Number	Time	Synoptic Wind Time	CALIOP period	Factor
1	00:00 - 03:00	00:00	night	1/8
2	03:00 - 06:00	06:00	night	1/8
3	06:00 - 09:00	06:00	day	1/8
4	09:00 - 15:00	12:00	day	2/8
5	15:00 - 18:00	18:00	day	1/8
6	18:00 - 21:00	18:00	night	1/8
7	21:00 - 00:00	00:00	night	1/8

In these maps, it is very noticeable that we have limited coverage. These maps show a non-gray colour, show deposition or production, where there is at least one month where we can calculate the deposition for that lat-lon during the stated period. For other lat-lons where we have multiple months with values of  $F_{ij}$ , we take a simple average of these. This highlights the extent of the masking; the gray areas in the figures are where we could not calculate a deposition rate at this lat-lon for any of the months within the time range. The source of this masking is from the coverage of the ORAC dust AOD and the CALIOP extinction profiles, we can only report data in areas where we have both. However the main cause of masking was from ORAC.

Excessive comes about since a masked lat-lon in the ORAC or CALIOP data lead to 5 or 50 masked lat-lons in the deposition data, since we need to know fluxes out of the cells neighbouring our lat-lon as well as out of this cell. This has the effect of contracting the boundary of available data by 1 point compared to the overlap of available data from ORAC and CALIPSO. This causes us to lose a lot of coverage.

Examining the deposition data that we have managed to extract, it appears to contain much noise. On average the uncertainty of  $F_{ij}$  is larger than its value. We also note that there appears to be some unphysical dust production, such as in figure 3 where we have emission of dust from regions in the Atlantic Ocean and Arabian sea. It is strange that we could get this result, however since the uncertainties are large, the uncertainty range almost always makes it possible for these areas of unphysical emission to be at least areas of zero emission.

We do generally have emission of dust from the Saharan region of North Africa, and from the Bodl depression. This can be seen with more clarity when the data is binned over larger lat-lon scales (see Appendix) but some of the inconsistencies of unphysical emission remain.

An additional feedback we could have employed would have been to find where in the columns the mass was being lost or created. However, with our analysis being completed in cloud free conditions, we do not not know how rainfall has actually affected the average extinction profile and AOD we are using. So although we could examine where in the mass is diverging, it would present us with little information about the physical validity of our analysis.

## 5.1 Historic Projection

One of the major advantages of the ORAC derived data is its early start date of 1995. This means that, since we have access to wind data from this period via ECWMF, if we can estimate an extinction profile, we can calculate the deposition rate for periods as far back as 1995. This could be useful in evaluating the deposition effect on historic algal blooms. In this project I attempted to estimate this, but I shant present any results here since once again the data contained much noise.

## 5.2 Limitations

It must be noted that there are some limitations of this data, which here I would like to address. First of all and perhaps most importantly is the effect of using monthly averages in the calculations instead

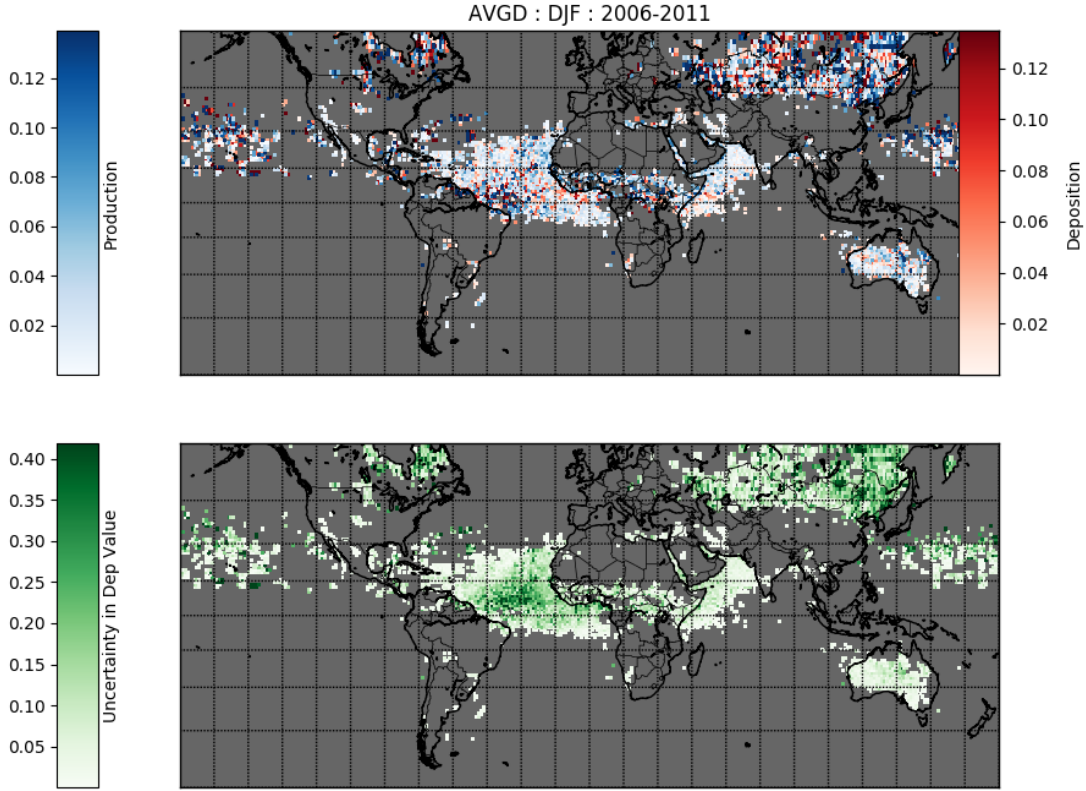


Figure 2: Average Deposition/Emission rate during the winter months (Dec, Jan, Feb) between Dec 2006 and Feb 2011. In the top plot areas of aerosol emission are in blue and areas of deposition are in red. Bottom plot shows the calculated uncertainty in the values, this is shown in green. Areas where data coverage was not available are shown in gray. Units are in  $Tg\ month^{-1}$  for each  $1^\circ \times 1^\circ$  cell.

of some higher time resolution. The reason this was chosen was due to the data available, taking daily data we can only cover a small swath of the planet, which, although more accurate since we can apply that day's wind fields, is of limited use when we wish to find seasonal fluxes. Ultimately the satellite sampling rate of the surface is too low to be able to hope to do this. Therefore we need to consider how using monthly averages of wind and dust load might effect results. It has to be noted that dust storms often happen on short scales, of order of a couple of days, where much of the aerosol dust load of the month will be concentrated. Therefore if the wind fields during this period are significantly different than their monthly averages we will have miscalculated the deposition. One correction we could apply without being able to sample the AOD more frequently could be to take the wind speeds from all days of the month and create a weighted monthly averaged wind speed. This could involve weighting winds in dust storm areas higher in days following a large dust storm and otherwise weighting at some base rate. This of course assumes that the wind speeds during these dust plumes deviate from the average, this may well be true, but more work would need to be done, since the dust storms themselves are products of extraordinary winds.

As mentioned before we may have some error due to assuming that the daytime AOD derived from ATSR is representative of the all time average.

Another thing that must be mentioned is that these calculation have all been derived from data that represents cloud-free observations. The CALIOP and the ORAC data are averages from times when each lat-lon was cloud free; meanwhile the wind data is from all times. This is an inconsistency

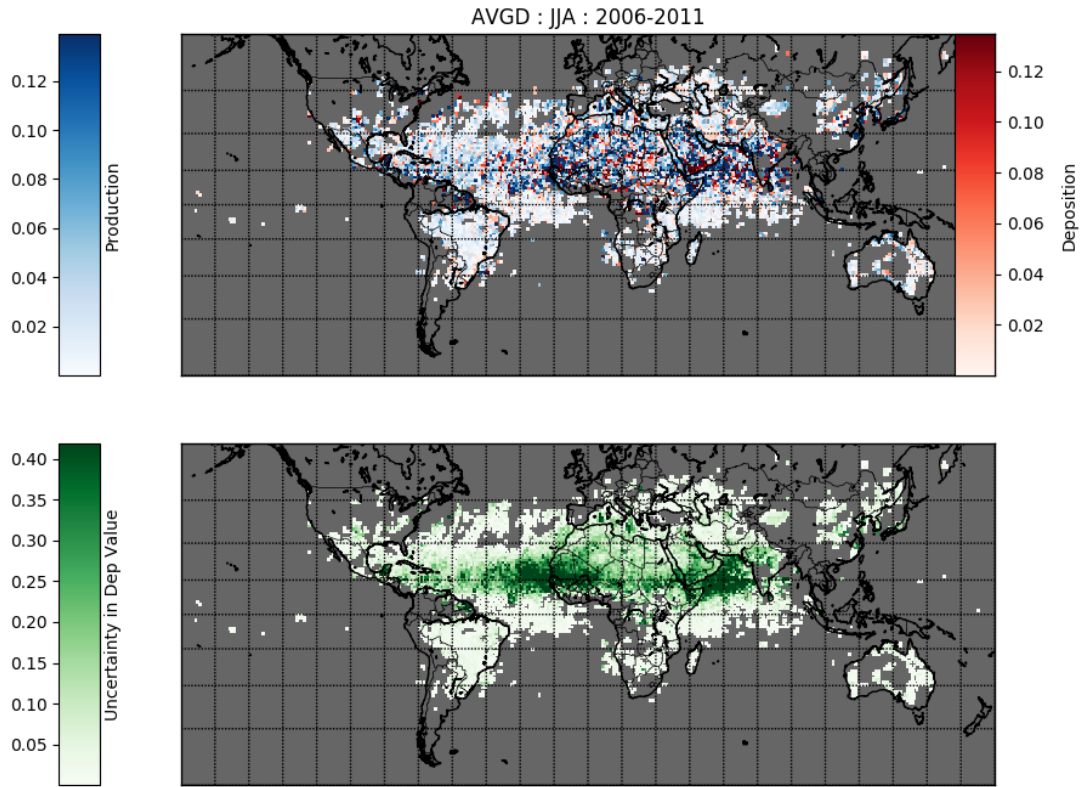


Figure 3: Average Deposition/Emission rate during the summer months (Jun, Jul, Aug) between Jun 2006 and Aug 2011. In the top plot areas of aerosol emission are in blue and areas of deposition are in red. Bottom plot shows the calculated uncertainty in the values, this is shown in green. Areas where data coverage was not available are shown in gray. Units are in  $Tg\ month^{-1}$  for each  $1^\circ \times 1^\circ$  cell.

and perhaps using cloud flags from the data we could accommodate for some better way to calculate an weighted average wind field. However there is a limitation to this still since it is below the clouds where much deposition may be taking place. Perhaps it would be possible to make some hybrid approach between the method laid out here and previous attempts to calculate the deposition using field measurements. Since the rain out deposition can be more easily evaluated than the dry deposition rate we could use the method presented here to evaluate dry deposition and an extrapolation of field measurements and precipitation to calculate wet deposition.

It also should be noted that the ORAC algorithm sometimes may flag very optically thick regions (such as a severe dust storm) as clouds, and so this falsely flagged data, if and where it exists, has been left out of our analysis.

We also note the limitations of using a single mass extinction efficiency. If this quantity significantly varies on spacial scales of less than  $1^\circ$  then we will undoubtedly have mischaracterised some regions of deposition as regions of emission and vice-versa. If it varies on scales larger than this then it will only be the magnitude of deposition/emission that is miscalculated.

I noted towards the end of this project that I was not fully utilising the information present within the datasets in evaluating the uncertainty. This I shall add to the appendix and the reader should note that the errors presented here are likely an overestimate as they were calculated in a simple manor from equation (4), without considering correlations and a non-diagonal variance-covariance matrix.

The presented errors also do not include many of the limitations given above.

## 6 Conclusions and Outlook

The aim of this project was to evaluate the dust aerosol deposition flux globally using major datasets already available. After searching through the literature I settled on a method that combined ECWMF wind, ORAC AOD and CALIOP extinction profile datasets to work out a deposition rate. What I found was a global deposition/emission rate of the order of  $0.1Tg\ month^{-1}$  per  $1^\circ \times 1^\circ$  global surface patch, which is consistent with earlier studies based on in site measurements, satellite flux analysis or climate models. There were limitations in the analysis in terms of differences in deposition between clear-sky and cloud conditions, there were also limitations in evaluating short-term dust storms and in general coverage of the earth's surface. I have proposed how one might correct for these first two limitations with average wind weighting and a hybrid satellite-field measurement method but this is beyond the scope of this study. I also note that there is a limitation in the absolute magnitude of the deposition rate due to the uncertainty in the mass extinction coefficient  $\Omega$  which has been estimated by laboratory experiments but which is predicted to vary downwind of dust sources. I suggested how one might use sediment trap data to accommodate for some of the spacial variance.

Ultimately the purpose of this study was to see how far this method of aerosol deposition calculation could be pushed and what potential there might be for further work. It is my belief, as I have presented in this paper, that some hybrid method could be adopted to remove some of the sources of error associated with this method but a major limiting factor in this is the aerosol AOD coverage. I considered some methods of filling edge values to improve the deposition coverage available, but I suspect more sophisticated methods could be used to evaluate this more carefully. I also note that the errors on the deposition are likely to be large (of order of magnitude of the data) no matter how the analysis is done due to uncertainty in the raw data.

## References

- [1] Hongbin Yu et al. "The fertilizing role of African dust in the Amazon rainforest: A first multi-year assessment based on data from Cloud-Aerosol Lidar and Infrared Pathfinder Satellite Observations". In: *Geophysical Research Letters* 42.6 (2015), pp. 1984–1991.
- [2] TD Jickells et al. "Global iron connections between desert dust, ocean biogeochemistry, and climate". In: *science* 308.5718 (2005), pp. 67–71.
- [3] Rachele Gallisai et al. "Saharan dust deposition may affect phytoplankton growth in the Mediterranean Sea at ecological time scales". In: *PLoS One* 9.10 (2014), e110762.
- [4] P Sedwick et al. "Assessing the Roles of Iron, Macronutrients and Wet deposition in Controlling Phytoplankton Growth in Seasonally Oligotrophic Waters of the Mid-Atlantic Bight". In: *American Geophysical Union, Ocean Sciences Meeting 2016, abstract# CT11A-03*. 2016.
- [5] Hanan Schoffman et al. "Iron–Nutrient Interactions within Phytoplankton". In: *Frontiers in plant science* 7 (2016).
- [6] Clara JM Hoppe et al. "Iron limitation modulates ocean acidification effects on Southern Ocean phytoplankton communities". In: *PloS One* 8.11 (2013), e79890.
- [7] X Meng et al. "Responses of phytoplankton community to the input of different aerosols in the East China Sea". In: *Geophysical Research Letters* 43.13 (2016), pp. 7081–7088.
- [8] Albert J Gabric et al. "Investigating the coupling between phytoplankton biomass, aerosol optical depth and sea-ice cover in the Greenland Sea". In: *Dynamics of Atmospheres and Oceans* 66 (2014), pp. 94–109.

- [9] Peter L Croot, Peter Streu, and Alex R Baker. “Short residence time for iron in surface seawater impacted by atmospheric dry deposition from Saharan dust events”. In: *Geophysical Research Letters* 31.23 (2004).
- [10] RA Duce et al. “The atmospheric input of trace species to the world ocean”. In: *Global biogeochemical cycles* 5.3 (1991), pp. 193–259.
- [11] DA Ridley, CL Heald, and B Ford. “North African dust export and deposition: A satellite and model perspective”. In: *Journal of Geophysical Research: Atmospheres* 117.D2 (2012).
- [12] Xiaohong Liu et al. “Global dust model intercomparison in AeroCom phase I”. In: *Atmospheric Chemistry and Physics* 11.15 (2011), p. 7781.
- [13] YJ Kaufman et al. “Dust transport and deposition observed from the Terra-Moderate Resolution Imaging Spectroradiometer (MODIS) spacecraft over the Atlantic Ocean”. In: *Journal of Geophysical Research: Atmospheres* 110.D10 (2005).
- [14] Ilan Koren et al. “The Bodélé depression: a single spot in the Sahara that provides most of the mineral dust to the Amazon forest”. In: *Environmental Research Letters* 1.1 (2006), p. 014005.
- [15] Hongbin Yu et al. “A satellite-based assessment of transpacific transport of pollution aerosol”. In: *Journal of Geophysical Research: Atmospheres* 113.D14 (2008).
- [16] Y Rudich et al. “Estimation of transboundary transport of pollution aerosols by remote sensing in the eastern Mediterranean”. In: *Journal of Geophysical Research: Atmospheres* 113.D14 (2008).
- [17] Hongbin Yu et al. “Aerosols from overseas rival domestic emissions over North America”. In: *Science* 337.6094 (2012), pp. 566–569.
- [18] Hongbin Yu et al. “Quantification of trans-Atlantic dust transport from seven-year (2007–2013) record of CALIPSO lidar measurements”. In: *Remote Sensing of Environment* 159 (2015), pp. 232–249.
- [19] Michèle van der Does et al. “Particle size traces modern Saharan dust transport and deposition across the equatorial North Atlantic”. In: *Atmospheric Chemistry and Physics* 16.21 (2016), p. 13697.
- [20] Laura F Korte et al. “Downward particle fluxes of biogenic matter and Saharan dust across the equatorial North Atlantic”. In: *Atmospheric Chemistry and Physics* 17.9 (2017), pp. 6023–6040.
- [21] Yung-Sung Cheng, Hsu-Chi Yeh, and Michael D Allen. “Dynamic shape factor of a plate-like particle”. In: *Aerosol science and technology* 8.2 (1988), pp. 109–123.
- [22] A Ansmann et al. “Profiling of fine and coarse particle mass: case studies of Saharan dust and Eyjafjallajökull/Grimsvötn volcanic plumes”. In: *Atmospheric Chemistry and Physics* 12.20 (2012), pp. 9399–9415.
- [23] Ilan Koren and Yoram J Kaufman. “Direct wind measurements of Saharan dust events from Terra and Aqua satellites”. In: *Geophysical research letters* 31.6 (2004).

# Appendices

## A Error Analysis

**Normalised Extinction Profile -  $\hat{b}_{ijk}$**  The error on  $\hat{b}_{ijk}$  can be calculated by considering the unnormalised  $b_{ijk}$  to be the product  $b_{ijk} = B_{ij}\hat{b}_{ijk}$  where  $B_{ij} = \sum_k b_{ijk}$ . Using standard error propagation this gives the uncertainty

$$\Delta\hat{b}_{ijk} = \frac{1}{B_{ij}}((\Delta b_{ijk})^2 - \hat{b}_{ijk}^2(\Delta B_{ij})^2)^{0.5} \quad (6)$$

where  $\Delta\hat{b}_{ijk}$  is the error in  $\hat{b}_{ijk}$ ,  $\Delta b_{ijk}$  is the error in  $b_{ijk}$  and  $\Delta B_{ij} = (\sum_k (\Delta b_{ijk})^2)^{0.5}$  is the error in  $B_{ij}$ .

This was the dominant source of uncertainty in our calculations as  $\Delta\hat{b}_{ijk}$  is generally larger than the value  $|\hat{b}_{ijk}|$ .

**Deposition Rate -  $F_{ij}$**  Calculating the error on the deposition rate is obviously more difficult than the calculation above and therefore I shall break it down into its subsequent parts, noting that the full error is given by,

$$\begin{aligned} (\Delta F_{ij})^2 = & \sum_{n \in N, m \in M, k} \left( \frac{\partial F_{ij}}{\partial \hat{b}_{nmk}} \right)^2 (\Delta \hat{b}_{nmk})^2 + \sum_{n \in N, m \in M, k} \left( \frac{\partial F_{ij}}{\partial V_{nmk}} \right)^2 (\Delta V_{nmk})^2 \\ & + \sum_{n \in N, m \in M, k} \left( \frac{\partial F_{ij}}{\partial U_{nmk}} \right)^2 (\Delta U_{nmk})^2 + \sum_{n \in N, m \in M} \left( \frac{\partial F_{ij}}{\partial A_{nm}} \right)^2 (\Delta A_{nm})^2 \\ & + \left( \frac{\partial F_{ij}}{\partial \Omega} \right)^2 (\Delta \Omega)^2, \end{aligned} \quad (7)$$

where we allow  $k$  to sum over all values and  $N = [i, i-1, i+1]$  and  $M = [j, j-1, j+1]$ . We can express each of these parts as in equation (4). Below we evaluate each of the terms in the equation above individually. This is a straight assuming the variance-covariance matrix is diagonal.

The uncertainty caused by the extinction coefficient,

$$\begin{aligned} \sum_{n \in N, m \in M, k} \left( \frac{\partial F_{ij}}{\partial \hat{b}_{nmk}} \right)^2 (\Delta \hat{b}_{nmk})^2 = & \frac{1}{\Omega^2} \{ \\ & \sum_k \left\| \oplus A_{i,j} \text{sign}(\hat{b}_{ijk}) U_{ijk} L_{ij}^{u+} \right\|^2 (\Delta \hat{b}_{ijk})^2 + \left\| \ominus A_{i,j} \text{sign}(\hat{b}_{ijk}) U_{ijk} L_{ij}^{u-} \right\|^2 (\Delta \hat{b}_{ijk})^2 \\ & \sum_k \left\| \oplus A_{i,j} \text{sign}(\hat{b}_{ijk}) V_{ijk} L_{ij}^{v+} \right\|^2 (\Delta \hat{b}_{ijk})^2 + \left\| \ominus A_{i,j} \text{sign}(\hat{b}_{ijk}) V_{ijk} L_{ij}^{v-} \right\|^2 (\Delta \hat{b}_{ijk})^2 \\ & + \sum_k (\oplus A_{i-1,j} \text{sign}(\hat{b}_{i-1,jk}) V_{i-1,jk} L_{ij}^{v-})^2 (\Delta \hat{b}_{i-1,j,k})^2 \\ & + \sum_k (\ominus A_{i+1,j} \text{sign}(\hat{b}_{i+1,jk}) V_{i+1,jk} L_{ij}^{v+})^2 (\Delta \hat{b}_{i+1,j,k})^2 \\ & + \sum_k (\oplus A_{i,j-1} \text{sign}(\hat{b}_{i,j-1,k}) U_{i,j-1,k} L_{ij}^{u-})^2 (\Delta \hat{b}_{i,j-1,k})^2 \\ & + \sum_k (\ominus A_{i,j+1} \text{sign}(\hat{b}_{i,j+1,k}) U_{i,j+1,k} L_{ij}^{u+})^2 (\Delta \hat{b}_{i,j+1,k})^2 \\ & \}. \end{aligned} \quad (8)$$

The uncertainty caused by the wind, U,

$$\begin{aligned}
\sum_{n \in N, m \in M, k} \left( \frac{\partial F_{ij}}{\partial U_{nmk}} \right)^2 (U_{nmk})^2 &= \frac{1}{\Omega^2} \{ \\
&\sum_k \left\| \oplus A_{i,j} \hat{b}_{ijk} \text{sign}(U_{ijk}) L_{ij}^{u+} \right\|^2 (\Delta U_{ijk})^2 + \left\| \ominus A_{i,j} \hat{b}_{ijk} \text{sign}(U_{ijk}) L_{ij}^{u-} \right\|^2 (\Delta U_{ijk})^2 \\
&\quad + \sum_k (\oplus A_{i,j-1} \hat{b}_{i,j-1,k} \text{sign}(U_{i,j-1,k}) L_{ij}^{u-})^2 (\Delta U_{i,j-1,k})^2 \\
&\quad + \sum_k (\ominus A_{i,j+1} \hat{b}_{i,j+1,k} \text{sign}(U_{i,j+1,k}) L_{ij}^{u+})^2 (\Delta U_{i,j+1,k})^2 \\
&\quad \left. \vphantom{\sum_k} \right\}. \quad (9)
\end{aligned}$$

The uncertainty caused by the wind, V,

$$\begin{aligned}
\sum_{n \in N, m \in M, k} \left( \frac{\partial F_{ij}}{\partial V_{nmk}} \right)^2 (\Delta V_{nmk})^2 &= \frac{1}{\Omega^2} \{ \\
&\sum_k \left\| \oplus A_{i,j} \hat{b}_{ijk} \text{sign}(V_{ijk}) L_{ij}^{v+} \right\|^2 (\Delta V_{ijk})^2 + \left\| \ominus A_{i,j} \hat{b}_{ijk} \text{sign}(V_{ijk}) L_{ij}^{v-} \right\|^2 (\Delta V_{ijk})^2 \\
&\quad + \sum_k (\oplus A_{i-1,j} \hat{b}_{i-1,j,k} \text{sign}(V_{i-1,j,k}) L_{ij}^{v-})^2 (\Delta V_{i-1,j,k})^2 \\
&\quad + \sum_k (\ominus A_{i+1,j} \hat{b}_{i+1,j,k} \text{sign}(V_{i+1,j,k}) L_{ij}^{v+})^2 (\Delta V_{i+1,j,k})^2 \\
&\quad \left. \vphantom{\sum_k} \right\}. \quad (10)
\end{aligned}$$

The uncertainty caused by the AOD,

$$\begin{aligned}
\sum_{n \in N, m \in M} \left( \frac{\partial F_{ij}}{\partial A_{nm}} \right)^2 (\Delta A_{nm})^2 &= \frac{1}{\Omega^2} \{ \\
&\sum_k \left\| \oplus \hat{b}_{ijk} U_{ijk} L_{ij}^{u+} \right\|^2 (\Delta A_{ij})^2 + \left\| \ominus \hat{b}_{ijk} U_{ijk} L_{ij}^{u-} \right\|^2 (\Delta A_{ij})^2 \\
&\sum_k \left\| \oplus \hat{b}_{ijk} V_{ijk} L_{ij}^{v+} \right\|^2 (\Delta A_{ij})^2 + \left\| \ominus \hat{b}_{ijk} V_{ijk} L_{ij}^{v-} \right\|^2 (\Delta A_{ij})^2 \\
&\quad + \sum_k (\oplus \hat{b}_{i-1,j,k} V_{i-1,j,k} L_{ij}^{v-})^2 (\Delta A_{i-1,j})^2 \\
&\quad + \sum_k (\ominus \hat{b}_{i+1,j,k} V_{i+1,j,k} L_{ij}^{v+})^2 (\Delta A_{i+1,j})^2 \\
&\quad + \sum_k (\oplus \hat{b}_{i,j-1,k} U_{i,j-1,k} L_{ij}^{u-})^2 (\Delta A_{i,j-1})^2 \\
&\quad + \sum_k (\ominus \hat{b}_{i,j+1,k} U_{i,j+1,k} L_{ij}^{u+})^2 (\Delta A_{i,j+1})^2 \\
&\quad \left. \vphantom{\sum_k} \right\}. \quad (11)
\end{aligned}$$

The uncertainty caused by the mass extinction coefficient,

$$\begin{aligned}
\left(\frac{\partial F_{ij}}{\partial \Omega}\right)^2 (\Delta \Omega)^2 &= \frac{(\Delta \Omega)^2}{\Omega^4} \{ \\
&- \sum_k \left\| \oplus A_{i,j} \hat{b}_{ijk} U_{ijk} L_{ij}^{u+} \right\| + \left\| \ominus A_{i,j} \hat{b}_{ijk} U_{ijk} L_{ij}^{u-} \right\| + \left\| \oplus A_{i,j} \hat{b}_{ijk} V_{ijk} L_{ij}^{v+} \right\| + \left\| \ominus A_{i,j} \hat{b}_{ijk} V_{ijk} L_{ij}^{v-} \right\| \\
&\quad + \sum_k \oplus A_{i-1,j} \hat{b}_{i-1,jk} V_{i-1,jk} L_{ij}^{v-} \\
&\quad + \sum_k \ominus A_{i+1,j} \hat{b}_{i+1,jk} V_{i+1,jk} L_{ij}^{v+} \\
&\quad + \sum_k \oplus A_{i,j-1} \hat{b}_{i,j-1,k} U_{i,j-1,k} L_{ij}^{u-} \\
&\quad + \sum_k \ominus A_{i,j+1} \hat{b}_{i,j+1,k} U_{i,j+1,k} L_{ij}^{u+} \\
&\quad \left. \right\}^2. \quad (12)
\end{aligned}$$

## B Better Error Analysis

There are some problems with the above error analysis, which having left Oxford now I am unable to correct. The first of which comes from differentiating terms of the form  $\oplus f(x)$  where  $f(x)$  is a generic function,  $x$  a variable, and the operator *oplus*, as before, adds the term to follow if it is positive and does nothing otherwise. This is a clumsy expression and should better be expressed via a function like

$$\oplus(f(x)) = \begin{cases} x, & \text{if } f(x) > 0 \\ 0, & \text{otherwise} \end{cases} \quad (13)$$

Note that the function  $\oplus$  is essentially a Heavyside-step function multiplied by its argument. When propagating an uncertainty through this I have used

$$\sigma_x^2 = \left( \frac{\partial \oplus(f(x))}{\partial x} \right)^2 (\Delta x)^2 = \oplus(\text{sign}(x) \partial f(x) / \partial x)^2 (\Delta x)^2.$$

I now do not believe this is correct and that instead the variance should map  $\sigma_x^2 \rightarrow \tilde{\oplus}^2(f(x), \Delta x)$  where

$$\tilde{\oplus}(f(x), \Delta x) = \begin{cases} \left| \frac{\partial f(x)}{\partial x} \right| \Delta x, & \text{if } f(x) > 0 \\ \left| \frac{\partial f(x)}{\partial x} \right| \Delta x + f(x), & \text{if } f(x) < 0 \text{ and } \left| \frac{\partial f(x)}{\partial x} \right| \Delta x + f(x) > 0 \\ 0, & \text{otherwise.} \end{cases} \quad (14)$$

The above expression takes into account places where we think the mass should be flowing in one direction, but the uncertainty in the calculated flow means that it could in fact be flowing in the opposite direction. We did not take this into account before and put a hard limit on this, we did not propagate the errors where the flow could be going in the reverse direction of the central value. We could make a similar substitution to handle the errors of  $\ominus$ .

Even the above correction is only an approximation since the uncertainty in the flow rate into any column, in reality, is not symmetric.

The second problem in this equation is in how we account propagate the error from the normalised extinction profile into  $F_{ij}$  in equation (8). In this equation we have overcompensated for the error associated with  $\hat{b}_{ijk}$ ; this can be seen if you imagine a wind field which is uniform in each column such that  $V_{ijk}(U_{ijk}) = V_{ij0}(U_{ij0})$ . In this case the contribution to the uncertainty due to  $\hat{b}_{ijk}$  should be zero

since we know the mass at every level is flowing with the same velocity. Therefore it doesn't matter how the mass is dispersed in the column, only what the total mass is, this is dependant on  $A_{ij}$  and  $\Omega$  but not  $\hat{b}_{ijk}$ . However this is not the result that equation (8) would give in this case; it should give zero but it does not. Further cases where there is only a little variation in the wind in the column will overcalculate the error as well. Generally, we find that the winds are correlated in the mass column at the heights of aerosol dust and flow in a preferred direction, this means there is correlation in the terms of the equation and that the variance-covariance matrix is not diagonal.

These are problems that have not been fully addressed and would take more time to solve. Therefore, they remain in the data.

## C Extra Plots

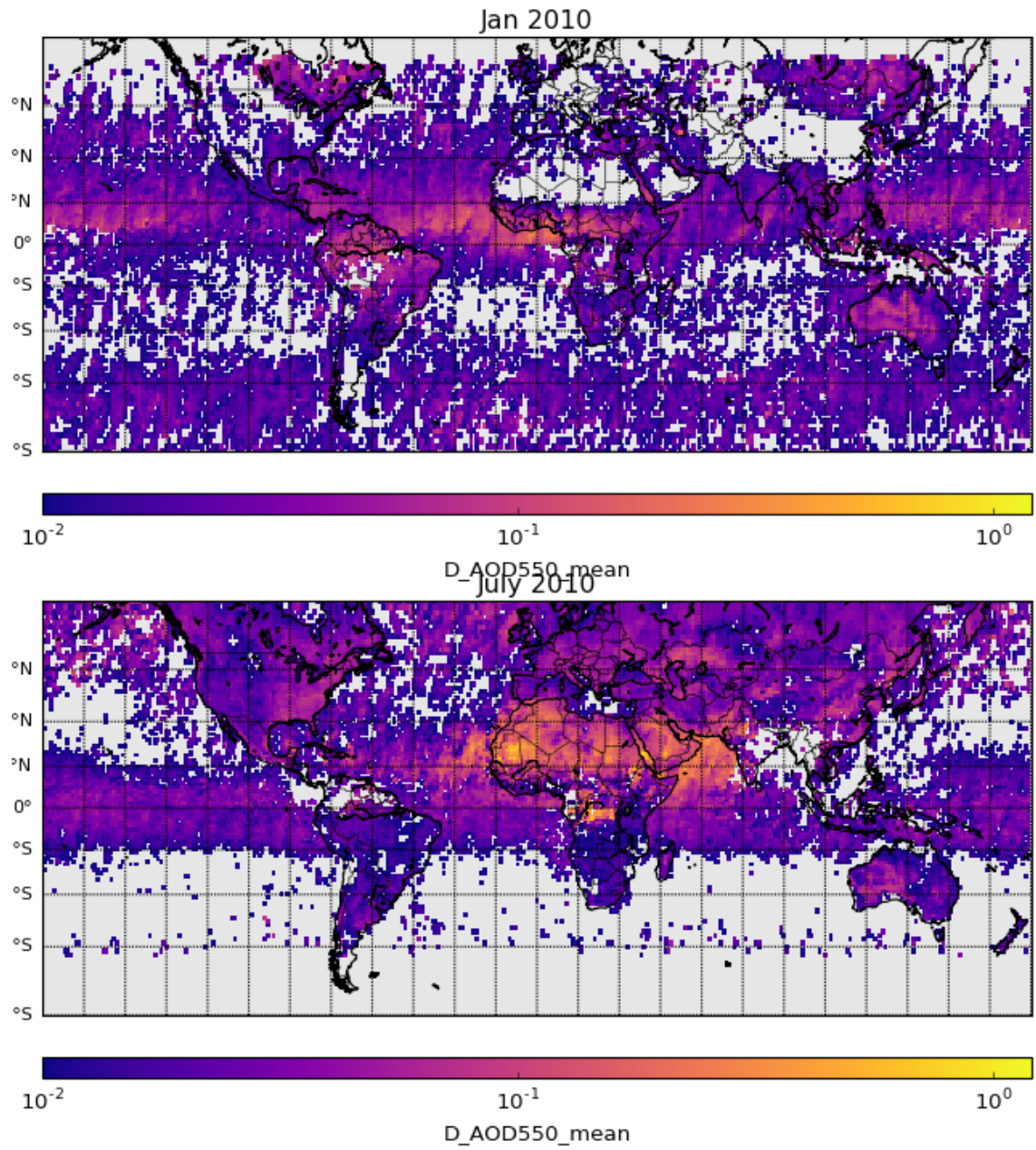


Figure 4: Aerosol Optical depth as retrieved by the ORAC algorithm for January and July 2010. We note here the strange seasonal variation in available coverage of data, particularly over the Sahara which was a limiting feature on our analysis. We also note that the ORAC AOD, disregarding the spatial variance is consistent with a field value. Around 70% of the dust AOD values lie within their uncertainty of the mean field value.

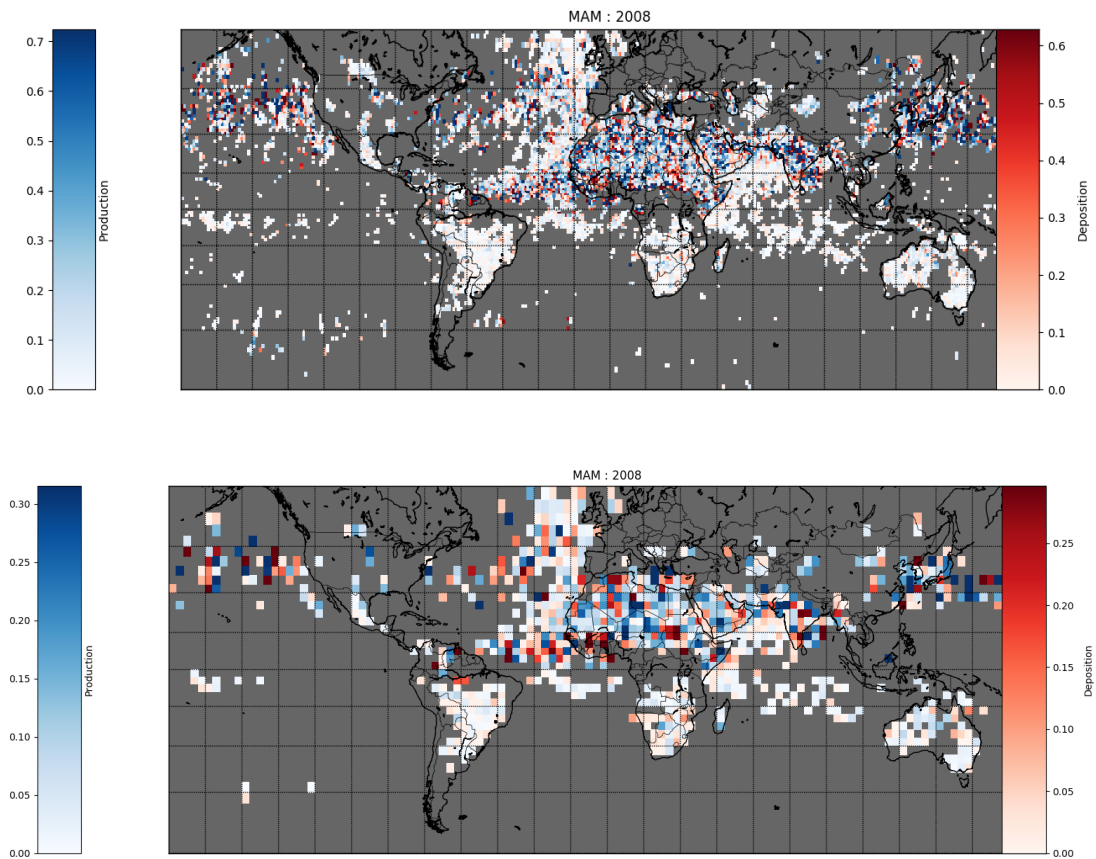


Figure 5: Average Deposition/Emission rate during spring 2008. Areas of aerosol emission are in blue and areas of deposition are in red. The top plot shows the deposition flux binned onto  $1^\circ \times 1^\circ$  columns whilst the bottom plot shows it binned onto  $3^\circ \times 3^\circ$  columns. Areas where data coverage was not available are shown in gray. Units are in  $Tg\ month^{-1}$  for each  $1^\circ \times 1^\circ$  cell. In the bottom plot it is easier to see that there is a high amount of dust production over the Sahara.

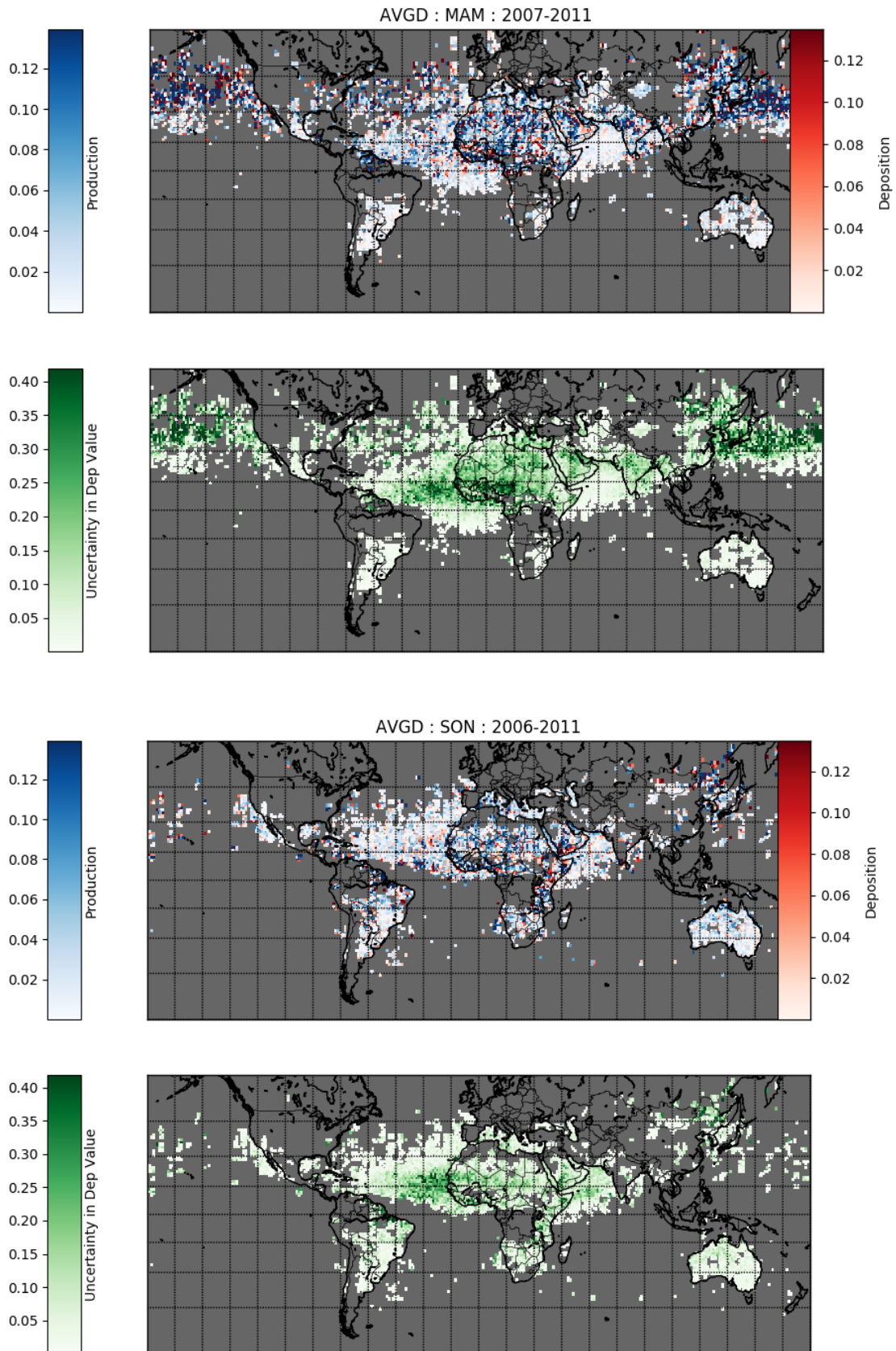


Figure 6: Figures for the missing seasons of spring and autumn. These are plotted in an identical manor to figs 2 and 3.